Large Diamagnetism and Electromagnetic Duality in Two-Dimensional Dirac Electron System

S. Fujiyama,[1,*] H. Maebashi,[2,†] N. Tajima,[3] T. Tsumuraya,[4] H-B. Cui,[1] M. Ogata,[2,5] and R. Kato[1]
[1]RIKEN, Condensed Molecular Materials Laboratory, Wako 351-0198, Japan
[2]Department of Physics, University of Tokyo, Tokyo 113-0033, Japan
[3]Department of Physics, Toho University, Funabashi 274-8510, Japan
[4]POIE, Kumamoto University, Kumamoto 860-8555, Japan
[5]Trans-scale Quantum Science Institute, University of Tokyo, Bunkyo-ku, Tokyo 113-0033, Japan

(Received 5 May 2021; accepted 21 December 2021; published 12 January 2022)

A Dirac electron system in solids mimics relativistic quantum physics that is compatible with Maxwell's equations, with which we anticipate unified electromagnetic responses. We find a large orbital diamagnetism only along the interplane direction and a nearly temperature-independent electrical conductivity of the order of e^2/h per plane for the new 2D Dirac organic conductor, α-$(BETS)_2I_3$, where BETS is bis(ethylenedithio)tetraselenafulvalene. Unlike conventional electrons in solids whose nonrelativistic effects bifurcate electric and magnetic responses, the observed orbital diamagnetism scales with the electrical conductivity in a wide temperature range. This demonstrates that an electromagnetic duality that is valid only within the relativistic framework is revived in solids.

DOI: 10.1103/PhysRevLett.128.027201

Dirac electron systems (DESs) such as bismuth and graphene can be described by the Dirac equation and provide a platform to realize physical properties rooted in relativistic quantum physics [1,2]. One prominent property of DESs is their large orbital diamagnetism, which reaches a maximum when the chemical potential is in the mass gap, unlike Landau diamagnetism in metals. This orbital diamagnetism, which is theoretically argued to originate from the interband effect of magnetic fields, is observed in three-dimensional (3D) DESs including bismuth and antiperovskites [3–6]. This mechanism also applies to two-dimensional (2D) systems. The diamagnetism was observed for mass-produced graphene flakes [7]. Here, the random orientation of the flakes prevented separating the orbital diamagnetism agreeable with theory. Organic conductors have recently been found to realize 2D DESs with a bulk form such as α-(BEDT-TTF)$_2$I$_3$ (BEDT-TTF = bis(ethylene)dithiotetrathiafulvalene) [8–10]; however, this is realized only under high pressure, limiting magnetic experiments and making it difficult to obtain the absolute value of the susceptibility using superconducting quantum interference device (SQUID) magnetometers.

The electric responses of 3D and 2D DESs show a sharp contrast. The uniform permittivity of bismuth is enhanced in accordance with its orbital diamagnetism [11,12]. On the other hand, graphene has no enhancement in the permittivity but rather shows exotic quantized optical conductance and minimum dc conductivity through Klein tunneling [2,13,14]. The organic conductor α-(BEDT-TTF)$_2$I$_3$ also shows temperature-independent conductivity on the order of e^2/h per sheet [15].

These magnetic and electric responses of DESs can be viewed as parallel to quantum electrodynamics (QED), a relativistic quantum field theory, in which two responses are unified due to the Lorentz covariance (spacetime symmetry). Indeed, for 3D DESs, the large orbital diamagnetism and the enhanced permittivity can be explained by charge renormalization in a unified way, demonstrating an electromagnetic duality specified by the spacetime symmetry of the Dirac equation [16]. In contrast to 3D DESs, permittivity enhancement due to charge renormalization is absent in 2D DESs [17], although they do exhibit a quantized conductance. The dependence of the charge renormalization on the dimensionality of the system raises the fundamental question of the existence and nature of the universal phenomena in DESs irrespective of the system dimension. Therefore, the two principal goals of the study of 2D DESs are to determine the behavior of the orbital diamagnetism and its relationship with quantized electric responses, and to clarify whether the two responses can be described by a unified theory. Observation of the orbital diamagnetism would resolve these questions, and in order to obtain absolute values of the magnetic susceptibility, a bulk-form single crystal at ambient pressure would be ideal.

In this Letter, we demonstrate the magnetic and transport properties of a newly identified 2D DES organic conductor with a bulk form at ambient pressure, α-$(BETS)_2I_3$ with a strongly anisotropic magnetic susceptibility χ. We discriminated a large orbital diamagnetism ($\chi_{\rm orb}$) from a spin susceptibility ($\chi_{\rm spin}$) by changing the field direction. $\chi_{\rm orb}$ shows quantitative agreement with the theory for $T > 50$ K, where the dc conductivity ($\sigma_{\rm dc}$) per sheet is independent of

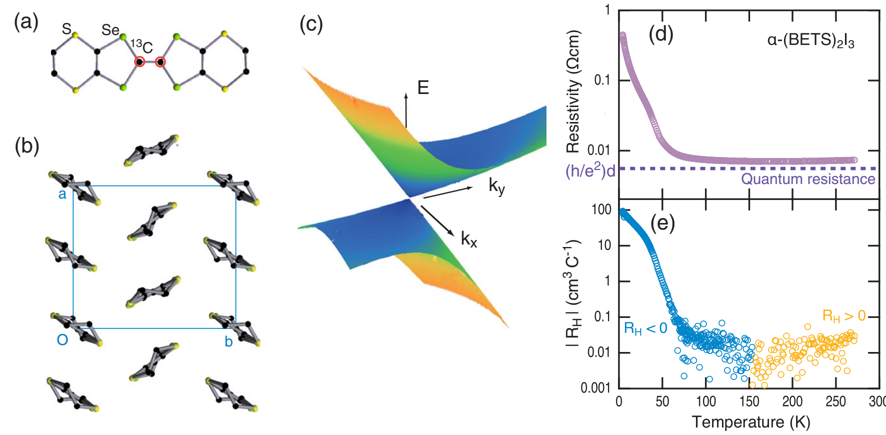

FIG. 1. (a) Molecular structure of bis(ethylenedithio)tetraselenafulvalene (BETS). Carbon atoms encircled in red are labeled by ^{13}C for NMR experiments. (b) Molecular arrangement of conducting plane of α-(BETS)$_2$I$_3$. (c) Dirac cone band dispersions calculated by *ab initio* method. (d) Resistivity at ambient pressure. The bulk resistivity corresponding to the quantum sheet resistance, $(h/e^2)d$, is shown as the dashed line. (e) Absolute values of the Hall coefficient.

temperature with the value of e^2/h. The $-T\chi_{\rm orb}$ scales with $\sigma_{\rm dc}$ in a wide temperature range, showing an electromagnetic duality specified by the spacetime symmetry in DESs, corresponding to the Lorentz covariance in QED.

α-(BETS)$_2$I$_3$ is composed of bis(ethylenedithio)tetraselenafulvalene (BETS) molecules that contain Se atoms [Fig. 1(a)] [18,19]. The structure is isomorphous with α-(BEDT-TTF)$_2$I$_3$, as shown in Fig. 1(b). The molecular orbital of BETS is spatially larger than that of BEDT-TTF, which yields uncorrelated electron characteristics and prevents the instabilities toward charge ordering or excitonic orders observed in α-(BEDT-TTF)$_2$I$_3$ [20]. This noninteracting character enables us to extract the ideal physics of DES through theoretical and quantitative analysis.

The full relativistic first-principles calculation provides a Dirac-like linear dispersion with a mass gap of $\approx$2 meV [Fig. 1(c)] and an effective "speed of light" of $v \approx 5 \times 10^4$ m/s [21–24]. The resistivity above 50 K is nearly independent of temperature, as has also been observed in the high-pressure massless Dirac phase of α-(BEDT-TTF)$_2$I$_3$ [Fig. 1(d)]. Here, Dirac electrons compensate for the temperature dependence of the mobility and the density of states [8], resulting in the temperature-independent resistivity corresponding to quantum sheet resistance, $(h/e^2)d = 4.6$ mΩ cm, where $d = 17.8$ Å is the interplane distance using the value of the lattice constant along c.

The resistivity increases upon cooling below 50 K without a phase transition, consistent with the mass gap, but does not follow an activated temperature dependence. The Hall coefficient (R_H) is small above 50 K, and its sign changes at $T = 150$ K from high-temperature positive (holelike) values to low-temperature negative (electronlike) values, as shown in Fig. 1(e). This indicates that the Fermi

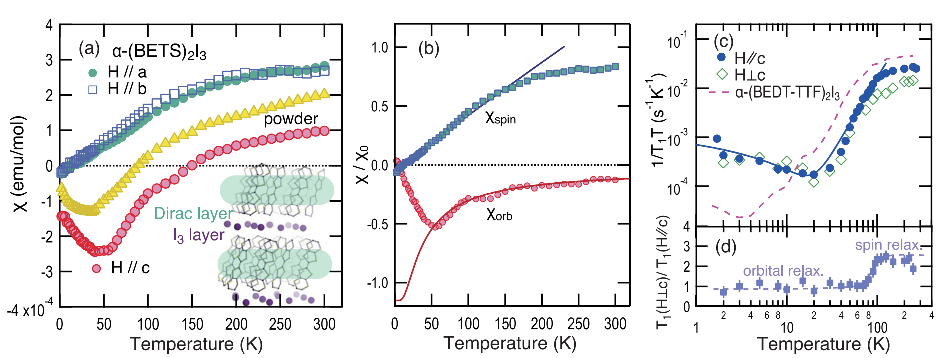

FIG. 2. Magnetic properties of α-(BETS)$_2$I$_3$. (a) Magnetic susceptibilities (χ) of a single crystal measured for $H\|a$, b, and c directions and polycrystalline samples. In the inset, the hatched area is the ab-plane hosting the 2D Dirac electrons isolated by anion (I$_3$) layers. (b) Spin ($\chi_{\rm spin}$) and orbital ($\chi_{\rm orb}$) susceptibilities scaled by $\chi_0 = \mu_0 e^2/2\pi m_0 d$. Solid curves are calculated susceptibilities for $\Delta = 50$ K using Eqs. (1) and (2). (c) Nuclear spin-lattice relaxation rate divided by temperature, $1/T_1T$, of ^{13}C NMR. The solid curve is a functional form of $1/T_1T = aT^{2.5} + b\log(T^*/T)$. The dashed curve of $1/T_1T$ for an organic DES, α-(BEDT-TTF)$_2$I$_3$, under high pressure is from Ref. [20]. (d) Ratios of $1/T_1$'s for $H\|c$ and $H\perp c$ calculated using data in (c).

energy is in the mass gap but shifts slightly with temperature. At 150 K, the Fermi energy will be exactly at the midpoint of the gap.

We show in Fig. 2(a) the magnetic susceptibilities $\chi_{a,b,c}$ for $H\|a$, b, and c (interplane direction). The susceptibility χ_a, which nearly agrees with χ_b, decreases linearly upon cooling below 150 K, consistent with Dirac-type linear dispersion. A possible in-plane anisotropy of χ originating from the tilting of the Dirac cone is negligible; therefore, we can consider that $\chi_{a,b}$ solely depends on the density of states and the electronic correlation is negligible. A detailed formula for the spin contribution to χ is given below using χ_0, the spin susceptibility of 2D nonrelativistic electron gas with the interplane distance d:

$$\chi_{\mathrm{spin}}(T)=\frac{m^*}{m_0}\chi_0\left(\frac{2}{\beta\Delta}\ln\left(2\cosh\frac{\beta\Delta}{2}\right)-\tanh\frac{\beta\Delta}{2}\right), \tag{1}$$

where m_0 is the electron mass, $\Delta=m^*v^2$ is the mass gap, and $\beta=1/k_BT$. $\chi_0=\mu_0e^2/2\pi m_0d=1.57\times10^{-7}$ in Systeme International (SI) units, where μ_0 is the vacuum permeability. The chemical potential μ is set to be zero for simplicity (see Ref. [21] for general μ). In Fig. 2(b), we plot χ_{spin} using $\Delta=50$ K, which provides $m^*=\Delta/v^2=0.3m_0$ with the *ab initio* value of v, as well as the experimental $\chi_{\mathrm{spin}}^{(\mathrm{exp})}=(\chi_a+\chi_b)/2$, and find that this simple formula quantitatively reproduces the experiments.

The magnetic susceptibility perpendicular to the conducting plane, χ_c, is strongly suppressed and shows negative values below 150 K, which indicates an orbital diamagnetism, $\chi_{\mathrm{orb}}^{(\mathrm{exp})}=\chi_c-\chi_{\mathrm{spin}}^{(\mathrm{exp})}$, that emerges only along the c direction. This diamagnetic χ_{orb} was theoretically predicted for 2D DESs [25,26]. In contrast to spins, which are conserved, the orbital currents that generate χ_{orb} are not conserved. In general, the susceptibility of a nonconserved quantity has a contribution from high-energy bands, $\chi_{\mathrm{orb}}^{(\mathrm{exp})}(\infty)$, which is independent of temperature and irrelevant to the Dirac band. We estimated $\chi_{\mathrm{orb}}^{(\mathrm{exp})}(\infty)$ by fitting $\chi_{\mathrm{orb}}^{(\mathrm{exp})}(T)$ for $T>100$ K with $\chi_{\mathrm{orb}}^{(\mathrm{exp})}(T)=\mathrm{const}\times1/T+\chi_{\mathrm{orb}}^{(\mathrm{exp})}(\infty)$ [see below Eq. (3)]. We plot in Fig. 2(b) the temperature-dependent component $\chi_{\mathrm{orb}}(T)=\chi_{\mathrm{orb}}^{(\mathrm{exp})}(T)-\chi_{\mathrm{orb}}^{(\mathrm{exp})}(\infty)$.

For free electrons, a detailed formula for $\chi_{\mathrm{orb}}(T)$ in the presence of a mass gap is given by [27]

$$\chi_{\mathrm{orb}}(T)=-\frac{2}{3}\frac{m_0}{m^*}\chi_0\tanh\frac{\beta\Delta}{2}, \tag{2}$$

where the chemical potential μ is set to be zero (see Ref. [21] for general μ). In Fig. 2(b), we plot experimental and calculated χ_{orb} obtained using Eq. (2) with the same parameters as those for χ_{spin}. We find quantitative agreements between the experimental and theoretical values as well as those for χ_{spin} in the wide temperature range of $T>50$ K. Equation (2) shows a crossover at $T\approx\Delta/k_B$ and is approximated as

$$\chi_{\mathrm{orb}}(T)=-\frac{2}{3}\frac{m_0v^2}{\max(\Delta,2k_{\mathrm{B}}T)}\chi_0 \tag{3}$$

so that $\chi_{\mathrm{orb}}T=\mathrm{const}$ is expected for $T\gtrsim\Delta/k_{\mathrm{B}}$.

The observed uncorrelated character of the 2D DES for $T>50$ K and the deviation of $\chi_{\mathrm{orb}}(T)$ from Eq. (2) are microscopically supported by ^{13}C NMR. High-temperature Korringa-like $1/T_1T$ for $T>200$ K is significantly reduced following $1/T_1T\propto T^\gamma$ with $\gamma\approx2$ for $30<T<100$ K as shown in Fig. 2(c), which indicates a linear dispersion. Note that the observed $1/T_1T$ is 5 times smaller than that of α-$(\mathrm{BEDT\text{-}TTF})_2\mathrm{I}_3$, showing that the Dirac electrons in α-$(\mathrm{BETS})_2\mathrm{I}_3$ are relatively free of one-body renormalization of Coulomb repulsions [20]. The increase in $1/T_1T$ below 20 K indicates other emergent relaxation mechanisms. Figure 2(d) depicts the anisotropies of $1/T_1$, which we expect to be temperature-independent when the spin contribution $(1/T_1)_{\mathrm{spin}}$ dominates $1/T_1$. The reduction of the anisotropy below 100 K, the onset temperature of the DES, coincides with that of $(1/T_1)_{\mathrm{spin}}$. Since ^{13}C does not couple with the electric field gradient, the most plausible source of the relaxation at low temperatures is the fluctuation of the orbital currents, which contributes to $1/T_1$ as $1/T_1=(1/T_1)_{\mathrm{spin}}+(1/T_1)_{\mathrm{orb}}$. Recent theories point out that $(1/T_1)_{\mathrm{orb}}$ dominates $1/T_1$ in 3D Weyl materials [28,29] but predict $(1/T_1T)_{\mathrm{orb}}\propto T$ for clean 2D DESs, which does not reproduce the experiments below 20 K [29]. Later, we will discuss a potential mechanism for the deviation related to χ_{orb}.

The correspondence between DES and QED relates Eq. (3) to the exotic quantized electric property in 2D DESs. In parallel to the Lorentz covariance in QED, we can show a duality between electric and magnetic responses in DES [21,30,31]. For $|\mu|\leq\Delta$ and $T=0$, the static magnetic susceptibility χ_{orb} is given exactly as

$$\chi_{\mathrm{orb}}=-\frac{2}{\pi}\left(\frac{v}{c}\right)^2\int_{2\Delta/\hbar}^{\infty}\frac{\sigma(\omega)}{\varepsilon_0\omega^2}d\omega, \tag{4}$$

where c and ε_0 are the speed of light and vacuum permittivity, respectively [21]. Here, $\sigma(\omega)$ is the dynamical electrical conductivity, which originates only from interband electron-hole excitations. Thus, this duality relation indicates that dynamical vacuum fluctuations (the creation and annihilation of virtual electron-hole pairs), or the interband effect across the mass gap, necessarily generate the orbital diamagnetism $\chi_{\mathrm{orb}}<0$.

A dimensional analysis gives $\sigma(\omega)\propto(e^2/h)(\omega/v)^{D-2}$ for the massless limit of $\Delta\to0$ in the D dimensions. In three dimensions ($D=3$), Eq. (4) leads to a logarithmic divergence in χ_{orb} for $\Delta\to0$, which corresponds to the

TABLE I. Electromagnetic responses of 3D and 2D DESs, which capture the salient nature of QED, i.e., the Lorentz covariance (spacetime symmetry) and charge renormalization. An electromagnetic duality resulting from the spacetime symmetry relates χ_{orb} to $\sigma(\omega)$ through Eq. (4). The permittivity $\varepsilon(q,\omega)$ is renormalized at $q=\omega=0$ as $\varepsilon(0,0)=Z_3^{-1}\varepsilon_0$, where Z_3 is the charge renormalization factor. The enhancement of $-\chi_{\mathrm{orb}}$ originates from the enhanced $\varepsilon(0,0)$ for 3D DESs, whereas that for 2D DESs takes place with $Z_3=1$. For finite temperatures, χ_{orb} and $\varepsilon(0,0)$ are given by replacing Δ by T. Details are given in Ref. [21].

	χ_{orb}	$\sigma(\omega\gg 2\Delta/\hbar)$	$\varepsilon(0,0)/\varepsilon_0=Z_3^{-1}$
3D	$\propto\ln\Delta$	$\approx(e^2/h)\omega/v$	$\propto-\ln\Delta$
2D	$\propto-1/\Delta$	$\approx e^2/hd$	1

well-known ultraviolet divergence in the charge renormalization of QED [16]. In two dimensions ($D=2$), on the other hand, there is no charge renormalization [17]. The large diamagnetism $\chi_{\mathrm{orb}}\propto-1/\Delta$ in Eq. (3) is therefore free from charge renormalization but closely linked to the ω-independent electrical conductivity for $\Delta\to 0$, where it takes a universal value of $\sigma_0=e^2/4\hbar d$ (quantized optical conductance) [14,32]. (In Table I, we summarize χ_{orb} and $\sigma(\omega)$ as well as the permittivity ε for 3D and 2D DESs.) More precisely, using a detailed formula for $\sigma(\omega)$ [32], we find that the duality relation, Eq. (4), expresses χ_{orb} in terms of the universal constant σ_0 as

$$\chi_{\mathrm{orb}}=-\frac{4}{3\pi}\left(\frac{v}{c}\right)^2\frac{\hbar}{\varepsilon_0\Delta}\sigma_0. \tag{5}$$

It is noteworthy that the conductivity unit σ_0 can be rewritten using the susceptibility unit χ_0 as $\sigma_0=(\pi^2/Z_0\lambda_e)\chi_0$, where $Z_0=\sqrt{\mu_0/\varepsilon_0}\approx 120\pi\ \Omega$ is the impedance of free space and $\lambda_e=h/m_0c$ is the Compton wavelength, leading to the equivalence of Eqs. (3) and (5). This equivalence shows that χ_{orb} scales with the universal electric conductance $\sigma_0 d\approx e^2/h$ even for finite temperatures.

The dc conductivity $\sigma_{\mathrm{dc}}\equiv\alpha\sigma_0$ (α is of the order of 1) is difficult to determine theoretically, depending on the characteristics of the disorder [33–36]. α is naively given as $\alpha=8/\pi^2$ [37] for 2D massless Dirac electrons but remains under debate for $T\neq 0$. The experimentally obtained values of σ_{dc}'s for organic DES, in contrast, are independent of temperature both for α-$(\mathrm{BETS})_2\mathrm{I}_3$ and α-$(\mathrm{BEDT\text{-}TTF})_2\mathrm{I}_3$; the σ_{dc} values are approximately equal to $\sigma_{\mathrm{dc}}=14\ \mathrm{k}\Omega^{-1}\,\mathrm{m}^{-1}$, corresponding to $\alpha\approx 4/\pi^2$ [15].

We plot $-\chi_{\mathrm{orb}}T$ and σ_{dc}, normalized by χ_0 and σ_0, respectively, in Fig. 3, and find that these electromagnetic responses are scaled in a wide temperature range, as anticipated from Eq. (5). The observed electromagnetic duality manifests itself in the correspondence with the Lorentz covariance in QED. The interband effect across the mass gap in the presence of electromagnetic fields characterizes the physical properties.

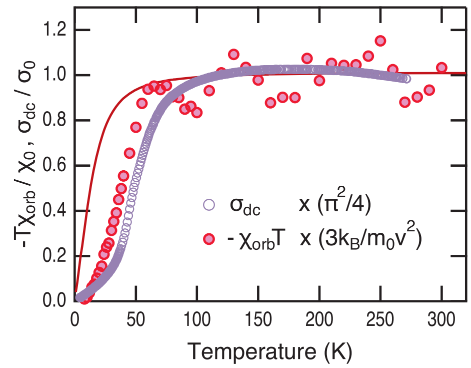

FIG. 3. Electromagnetic duality of α-$(\mathrm{BETS})_2\mathrm{I}_3$, where $-\chi_{\mathrm{orb}}T$ is scaled by σ_{dc} for a wide temperature range. The scaling factor is based on Eq. (3). The solid curve is the calculated $-\chi_{\mathrm{orb}}T$.

We now discuss potential sources for the deviation of $\chi_{\mathrm{orb}}(T)$ from Eq. (2), although Eq. (1) does reproduce $\chi_{\mathrm{spin}}(T)$ below 40 K. The most plausible source is a disorder in real materials, which raises a new problem related to the interaction of disorder and orbital currents in DESs. We found that the function $1/T_1T=aT^{2.5}+b\log(T^*/T)$ fits the $1/T_1T$, as shown in Fig. 2(c). The logarithmic increase upon cooling below 20 K does not originate from the electronic correlation, which enhances $1/T_1T$ for the whole temperature range, and the crossing of the $1/T_1T$ curves of α-$(\mathrm{BETS})_2\mathrm{I}_3$ and α-$(\mathrm{BEDT\text{-}TTF})_2\mathrm{I}_3$ at $T\approx 10$ K suggests disorder effects on $(1/T_1)_{\mathrm{orb}}$. A similar moderate increase of $1/T_1T$ is observed for a 3D Weyl system [38], which has been theoretically analyzed considering the effects of impurities or temperature-dependent chemical potential to $(1/T_1)_{\mathrm{orb}}$ [39,40]. Likewise, an observed increase in $1/T_1T$ for a noninteracting 3D DES with $\Delta\approx 15$ meV, $\mathrm{Bi}_{0.9}\mathrm{Sb}_{0.1}$ [41], is closely related to our observation of the moderate increase in $1/T_1T$ below 20 K. A related phenomenon is also observed for the transport properties: namely, unconventional negative magnetoresistance with a field dependence of the form $1-\rho(B)/\rho_0\propto-\sqrt{B}$ [21]. These deviations from an ideal 2D DES are observed solely for the orbital-related properties at low temperatures, which suggests a new problem in disordered orbital physics in DESs. Surprisingly, despite the deviation of χ_{orb} from Eq. (2) below 50 K, σ_{dc} approximately scales with $-\chi_{\mathrm{orb}}T$, thus maintaining the electromagnetic duality even at low temperatures where the effect of a disorder becomes crucial as shown in Fig. 3. This suggests a possible relationship between the effects of disorder on χ_{orb} and σ_{dc}, which results in a less disturbed electromagnetic duality.

In summary, we identified the organic conductor, α-$(\mathrm{BETS})_2\mathrm{I}_3$, as a 2D DES at ambient pressure through electric and magnetic measurements of σ_{dc}, R_H, χ_{spin}, and

$1/T_1$ of ^{13}C NMR. The latter two magnetic responses show negligible electronic correlation, enabling us to study an ideal characteristics of DES. We found orbital diamagnetism (χ_{orb}) only along the interplane direction. We demonstrate that the equation $T\chi_{\mathrm{orb}} = \mathrm{const}$ holds approximately for $T > 50$ K and $\chi_{\mathrm{spin}} \propto T$ and that small shifts from the gapless DES are well reproduced by the theory using a unique parameter, $\Delta = m^* v^2$, the mass gap for the DES. We found a unified electromagnetic responses in which $-T\chi_{\mathrm{orb}}$ scales with $\sigma_{\mathrm{dc}} \approx e^2/hd$ in a wide temperature range, as shown in Fig. 3, consistent with an electromagnetic duality that is valid only within the relativistic framework.

We are grateful to H. Fukuyama, H. Sawa, A. Kobayashi, T. Morinari, Y. Fuseya, H. Matsuura, I. Tateishi, and S. Ozaki for fruitful discussions. This work was supported by Grants-in-Aid for Scientific Research (20K03870, 21K03426, 18K03482, 18H01162, 19K21860, and 16H06346) from JSPS.

*Corresponding author.
fujiyama@riken.jp
†Corresponding author.
maebashi@hosi.phys.s.u-tokyo.ac.jp

[1] P. Wolff, Matrix elements and selection rules for the two-band model of bismuth, J. Phys. Chem. Solids **25**, 1057 (1964).
[2] K. S. Novoselov, A. K. Geim, S. V. Morozov, D. Jiang, M. I. Katsnelson, I. V. Grigorieva, S. V. Dubonos, and A. A. Firsov, Two-dimensional gas of massless Dirac fermions in graphene, Nature (London) **438**, 197 (2005).
[3] D. Shoenberg, M. Z. Uddin, and E. Rutherford, The magnetic properties of bismuth I Dependence of susceptibility on temperature and addition of other elements, Proc. R. Soc. A **156**, 687 (1936).
[4] L. Wehrli, Die magnetische Suszeptibilität von Bi und Bi-Sb-Legierungen, Phys. Kondens. Mater. **8**, 87 (1968).
[5] H. Fukuyama and R. Kubo, Interband effects on magnetic susceptibility. II. Diamagnetism of bismuth, J. Phys. Soc. Jpn. **28**, 570 (1970).
[6] S. Suetsugu, K. Kitagawa, T. Kariyado, A. W. Rost, J. Nuss, C. Mühle, M. Ogata, and H. Takagi, Giant orbital diamagnetism of three-dimensional Dirac electrons in Sr_3PbO antiperovskite, Phys. Rev. B **103**, 115117 (2021).
[7] Z. Li, L. Chen, S. Meng, L. Guo, J. Huang, Y. Liu, W. Wang, and X. Chen, Field and temperature dependence of intrinsic diamagnetism in graphene: Theory and experiment, Phys. Rev. B **91**, 094429 (2015).
[8] N. Tajima, M. Tamura, Y. Nishio, K. Kajita, and Y. Iye, Transport property of an organic conductor α-(BEDT-TTF)$_2$I$_3$ under high pressure—Discovery of a novel type of conductor -, J. Phys. Soc. Jpn. **69**, 543 (2000).
[9] S. Katayama, A. Kobayashi, and Y. Suzumura, Pressure-induced zero-gap semiconducting state in organic conductor α-(BEDT-TTF)$_2$I$_3$ salt, J. Phys. Soc. Jpn. **75**, 054705 (2006).
[10] M. Hirata, K. Ishikawa, K. Miyagawa, M. Tamura, C. Berthier, D. Basko, A. Kobayashi, G. Matsuno, and K. Kanoda, Observation of an anisotropic Dirac cone reshaping and ferrimagnetic spin polarization in an organic conductor, Nat. Commun. **7**, 12666 (2016).
[11] V. S. Édel'Man, Investigation of bismuth in a quantizing field, Sov. J. Exp. Theor. Phys. **41**, 125 (1975), http://www.jetp.ras.ru/cgi-bin/dn/e_041_01_0125.pdf.
[12] W. S. Boyle and A. D. Brailsford, Far infrared studies of bismuth, Phys. Rev. **120**, 1943 (1960).
[13] M. I. Katsnelson, K. S. Novoselov, and A. K. Geim, Chiral tunnelling and the Klein paradox in graphene, Nat. Phys. **2**, 620 (2006).
[14] Z. Q. Li, E. A. Henriksen, Z. Jiang, Z. Hao, M. C. Martin, P. Kim, H. L. Stormer, and D. N. Basov, Dirac charge dynamics in graphene by infrared spectroscopy, Nat. Phys. **4**, 532 (2008).
[15] N. Tajima, S. Sugawara, M. Tamura, R. Kato, Y. Nishio, and K. Kajita, Transport properties of massless Dirac fermions in an organic conductor α-(BEDT-TTF)$_2$I$_3$ under pressure, Europhys. Lett. **80**, 47002 (2007).
[16] H. Maebashi, M. Ogata, and H. Fukuyama, Lorentz covariance of Dirac electrons in solids: Dielectric and diamagnetic properties, J. Phys. Soc. Jpn. **86**, 083702 (2017).
[17] J. González, F. Guinea, and M. Vozmediano, Non-Fermi liquid behavior of electrons in the half-filled honeycomb lattice (A renormalization group approach), Nucl. Phys. **B424**, 595 (1994).
[18] M. Inokuchi, H. Tajima, A. Kobayashi, T. Ohta, H. Kuroda, R. Kato, T. Naito, and H. Kobayashi, Electrical and optical properties of α-(BETS)$_2$I$_3$ and α-(BEDT-TTF)$_2$I$_3$, Bull. Chem. Soc. Jpn. **68**, 547 (1995).
[19] K.-i. Hiraki, S. Harada, K. Arai, Y. Takano, T. Takahashi, N. Tajima, R. Kato, and T. Naito, Local Spin Susceptibility of α-D$_2$I$_3$ (D = bis(ethylendithio)tetraselenafulvalene (BETS) and bis(ethylendithio)dithiadiselenafulvalene (BEDT-STF)) Studied by ^{77}Se NMR, J. Phys. Soc. Jpn. **80**, 014715 (2011).
[20] M. Hirata, K. Ishikawa, G. Matsuno, A. Kobayashi, K. Miyagawa, M. Tamura, C. Berthier, and K. Kanoda, Anomalous spin correlations and excitonic instability of interacting 2D Weyl fermions, Science **358**, 1403 (2017).
[21] See Supplemental Material at http://link.aps.org/supplemental/10.1103/PhysRevLett.128.027201 for the experiments and band calculation methods, the procedure to estimate v, derivations of the equations for grneral μ, and the magnetoresistance data.
[22] S. Kitou, T. Tsumuraya, H. Sawahata, F. Ishii, K.-i. Hiraki, T. Nakamura, N. Katayama, and H. Sawa, Ambient-pressure Dirac electron system in the quasi-two-dimensional molecular conductor α-(BETS)$_2$I$_3$, Phys. Rev. B **103**, 035135 (2021).
[23] J. P. Perdew, K. Burke, and M. Ernzerhof, Generalized Gradient Approximation Made Simple, Phys. Rev. Lett. **77**, 3865 (1996).
[24] E. Wimmer, H. Krakauer, M. Weinert, and A. J. Freeman, Full-potential self-consistent linearized-augmented-plane-wave method for calculating the electronic structure of molecules and surfaces: O_2 molecule, Phys. Rev. B **24**, 864 (1981).
[25] J. W. McClure, Diamagnetism of graphite, Phys. Rev. **104**, 666 (1956).

[26] H. Fukuyama, Anomalous orbital magnetism and Hall effect of massless fermions in two dimension, J. Phys. Soc. Jpn. **76**, 043711 (2007).

[27] M. Koshino and T. Ando, Singular orbital magnetism of graphene, Solid State Commun. **151**, 1054 (2011).

[28] B. Dóra and F. Simon, Unusual Hyperfine Interaction of Dirac Electrons and NMR Spectroscopy in Graphene, Phys. Rev. Lett. **102**, 197602 (2009).

[29] H. Maebashi, T. Hirosawa, M. Ogata, and H. Fukuyama, Nuclear magnetic relaxation and Knight shift due to orbital interaction in Dirac electron systems, J. Phys. Chem. Solids **128**, 138 (2019).

[30] M. E. Peskin and D. V. Schroeder, *An Introduction to Quantum Field Theory* (Addison-Wesley, Reading, MA, 1995).

[31] G. F. Giuliani and G. Vignale, *Quantum Theory of the Electron Liquid* (Cambridge University Press, Cambridge, U.K., 2005).

[32] V. P. Gusynin, S. G. Sharapov, and J. P. Carbotte, Unusual Microwave Response of Dirac Quasiparticles in Graphene, Phys. Rev. Lett. **96**, 256802 (2006).

[33] N. H. Shon and T. Ando, Quantum transport in two-dimensional graphite system, J. Phys. Soc. Jpn. **67**, 2421 (1998).

[34] S. Adam, E. H. Hwang, V. M. Galitski, and S. Das Sarma, A self-consistent theory for graphene transport, Proc. Natl. Acad. Sci. U.S.A. **104**, 18392 (2007).

[35] P. M. Ostrovsky, I. V. Gornyi, and A. D. Mirlin, Electron transport in disordered graphene, Phys. Rev. B **74**, 235443 (2006).

[36] P. M. Ostrovsky, I. V. Gornyi, and A. D. Mirlin, Quantum Criticality and Minimal Conductivity in Graphene with Long-Range Disorder, Phys. Rev. Lett. **98**, 256801 (2007).

[37] T. Ando, Y. Zheng, and H. Suzuura, Dynamical conductivity and zero-mode anomaly in honeycomb lattices, J. Phys. Soc. Jpn. **71**, 1318 (2002).

[38] H. Yasuoka, T. Kubo, Y. Kishimoto, D. Kasinathan, M. Schmidt, B. Yan, Y. Zhang, H. Tou, C. Felser, A. Mackenzie *et al.*, Emergent Weyl Fermion Excitations in TaP Explored by Ta181 Quadrupole Resonance, Phys. Rev. Lett. **118**, 236403 (2017).

[39] T. Hirosawa, H. Maebashi, and M. Ogata, Nuclear spin relaxation rate near the disorder-driven quantum critical point in Weyl fermion systems, Phys. Rev. B **101**, 155103 (2020).

[40] Z. Okvátovity, H. Yasuoka, M. Baenitz, F. Simon, and B. Dóra, Nuclear spin-lattice relaxation time in TaP and the Knight shift of Weyl semimetals, Phys. Rev. B **99**, 115107 (2019).

[41] W. A. MacFarlane, C. B. L. Tschense, T. Buck, K. H. Chow, D. L. Cortie, A. N. Hariwal, R. F. Kiefl, D. Koumoulis, C. D. P. Levy, I. McKenzie, F. H. McGee, G. D. Morris, M. R. Pearson, Q. Song, D. Wang, Y. S. Hor, and R. J. Cava, β-detected NMR of $^8Li^+$ in Bi, Sb, and the topological insulator $Bi_{0.9}Sb_{0.1}$, Phys. Rev. B **90**, 214422 (2014).